



## **Environmental Impacts of Pastoral-Integrated Photovoltaic Power Plant in an Alpine Meadow on the Eastern Tibetan Plateau**

5    Shaoying Wang<sup>1, 2</sup>, Xianhong Meng<sup>1, 2</sup>, Qian Li<sup>3</sup>, Zhenchao Li<sup>1,2</sup>, Peipei Yang<sup>4</sup>,  
Wenzhen Niu<sup>5</sup>, Lunyu Shang<sup>1,2</sup>

<sup>1</sup>Key Laboratory of Cryospheric Science and Frozen Soil Engineering, Northwest  
10    Institute of Eco-Environment and Resources, Chinese Academy of Sciences, Lanzhou,  
730000, China.

<sup>2</sup>Zoige Plateau Wetlands Ecosystem Research Station, Northwest Institute of Eco-  
Environment and Resources, Chinese Academy of Sciences, Lanzhou, 730000, China.

<sup>3</sup>Shannxi Province Climate Center, Xi'an, 710014, China.

15    <sup>4</sup>State Grid Lanzhou Electric Power Supply Company, Lanzhou, 730000, China.

<sup>5</sup>Wuling Power Ningxia Representative Office.

*Correspondence to:* Shaoying Wang (wangshaoying@lzb.ac.cn), Qian Li  
(liqian2011@163.com)

20

25



**Abstract:** Rising global energy demand and the transition toward low-carbon energy sources have driven a rapid expansion of ground-mounted solar parks worldwide. This expansion constitutes a substantial land use change with largely unexplored implications for the ecosystems they occupy, particularly in the ecologically fragile and sensitive region of the Tibetan Plateau (TP). To assess the impacts of a typical photovoltaic (PV) power station on the alpine meadow ecosystem, this study conducted year-round observations of local microclimate and soil hydrothermal regimes within and adjacent to a pastoral-integrated PV plant on the eastern TP. The results show that PV installations significantly increase annual net radiation while reducing albedo and wind speeds. The influence of PV panels on air temperature is highly asymmetrical, with daytime heating, nighttime cooling, summer heating, and winter cooling. The PV arrays introduce notable spatial heterogeneity in soil hydrothermal regimes, show a cold-moist pattern in the array gaps and a cold-dry distribution beneath the panels. Such changes extend the frozen period and reduces soil moisture depletion rates. Our findings suggest that PV arrays could, in fact, enhance ecosystem resilience to climate warming; however, further research is needed to assess their impacts on hydrological processes, carbon balance, and biodiversity.

45

**Keywords:** Photovoltaic power plant, Alpine meadow, Microclimate, Soil hydrothermal dynamics, Field observations

50



## 55 1. Introduction

Photovoltaic (PV) power generation is a critical solution for addressing the global energy crisis, mitigating climate change, and reducing environmental pollution (Kan et al., 2021; Právělie et al., 2019). In recent decades, significant strides in the solar energy industry have been driven by the global transition from carbon-intensive fossil  
60 fuels to renewable energy and the rapid decline in solar PV costs (Wei et al., 2024). As the global leader in the photovoltaic industry, China has maintained its dominant position in PV power generation, with cumulative installed capacity accounting for approximately one-third of the global total (Biroi, 2022). In line with its carbon peaking and carbon neutrality goals, China is expected to continue rapidly expanding PV power  
65 generation nationwide.

Despite the clear advantages of PV power plants in clean energy production, their widespread deployment significantly alters local land surface properties and climate (Armstrong et al., 2016; Wei et al., 2024). These changes result primarily from the combined effects of surface roughness, the dark surfaces of PV panels, their energy  
70 output, and heat released during power generation (Broadbent et al., 2019; Taha, 2013; Xu et al., 2024; Yang et al., 2017). However, the environmental impacts of PV systems exhibit considerable regional variability, with studies reporting inconsistent trends and magnitudes of change depending on the local climate, ecosystem type, and PV array configuration.

75 For instance, PV arrays significantly influence albedo, a critical land surface parameter that directly influences the surface energy balance and climate dynamics (Wei et al., 2024). Numerical simulations often assume a simplified albedo value of 0.1 for PV arrays (Li et al., 2018; Lu et al., 2021), remote sensing and in-situ measurements typically report higher values, though with notable inconsistencies between the two  
80 methods (Chang et al., 2018; Li et al., 2022c; Wei et al., 2024; Xu et al., 2024; Yang et al., 2017). Similarly, PV plants influence near-surface air temperatures, most field studies indicate that PV panels increase daytime air temperatures due to heat released during electricity generation, a phenomenon similar to the urban heat island effect



(Armstrong et al., 2016; Broadbent et al., 2019; Fthenakis and Yu, 2013; Yang et al.,  
85 2017; Zheng et al., 2023). For example, Yang et al. (2017) showed that PV panels in  
desert areas can increase both daytime and nighttime 2m air temperatures by  
approximately 0.7°C and 0.1°C, respectively, due to the heat released during power  
generation and the heat retention effect near the ground. In arid regions of California,  
Barron-Gafford et al. (2016) found that PV panels raised summer 2.5m air temperatures  
90 by more than 3°C compared to nearby wildlands. However, Keiko et al. (2009)  
conducted research on large-scale PV power plants in desert regions and found that PV  
modules had a self-cooling mechanism at night, with temperatures 2–4°C lower than  
the surrounding atmospheric temperature when sunlight ceased. These significant  
variations in the environmental impacts of solar farms may be attributed to differences  
95 in their characteristics, such as type, spatial scale, capacity, installation methods, and  
background environmental conditions (Xu et al., 2024). These discrepancies highlight  
the need for observational studies to better understand the impacts of PV arrays across  
diverse climate zones and surface types.

The Tibetan Plateau (TP), known as the "Third Pole," is one of the most ecologically  
100 fragile regions on earth, playing a crucial role in global climate regulation. Its complex  
soil freeze-thaw dynamics, important water conservation functions, and substantial  
carbon release potential make it highly sensitive to environmental disturbances (Chen  
et al., 2016; Yao et al., 2022). Additionally, the TP's long daylight hours, high solar  
radiation intensity, low temperatures and vast areas create ideal natural conditions for  
105 the development of PV industries (Li et al., 2022a; Tang et al., 2013; Wang and Qiu,  
2009). In recent years, PV power plants have proliferated across the TP (Lyu et al.,  
2024), yet their impacts on microclimate and soil hydrothermal conditions, particularly  
in alpine meadows, remain underexplored. While extensive research exists on PV-  
induced microclimatic changes in deserts, a critical gap remains in understanding their  
110 effects on alpine ecosystems, which are both ecologically fragile and climate-sensitive.  
To address this gap, this study investigates the effects of a pastoral-integrated PV power  
plant on the microclimate and soil hydrothermal conditions of an alpine meadow on the  
eastern TP. Field observations were conducted at two neighboring sites within the



Dongneng PV solar park to monitor key variables, including air temperature, humidity,  
115 radiation balance, and soil hydrothermal conditions. The primary aim of this research  
is to evaluate and quantify the environmental impacts of PV plant deployment in this  
unique ecosystem, providing valuable insights into the environmental consequences of  
large-scale PV power generation. This work seeks to contribute to a deeper  
understanding of the environmental effects of renewable energy and offer insights for  
120 sustainable development as PV energy continues to expand.

## 2. Method

### 2.1 Site description

The Dongneng PV power plant (34°3'19.5"N, 101°53'17.6"E) is situated in Maqu,  
Gansu Province, on the eastern Tibetan Plateau at an altitude of 3440 m (Figure 01a).  
125 The region's climate is classified as a sub-frigid humid zone based on China's climate  
regionalization (Zheng et al., 2010). The nearest meteorological station, located  
approximately 15 km from the study site, recorded a mean annual precipitation of 607  
mm and an average air temperature of 1.84 °C from 1971 to 2020. The study area  
features alpine meadow vegetation dominated by *Stipa aliena*, *Potentilla anserina*, and  
130 *Scirpus pumilus*, with average vegetation heights of 0.3 m in summer and 0.1 m in  
winter. The PV power plant, located on flat terrain, was constructed in September 2021  
and became operational in August 2022. It has a capacity of 50 MW and utilizes bifacial  
photovoltaic panels (LONGi Green Energy Technology Co., Ltd.) with a photoelectric  
conversion efficiency of 21.1%. The arrays are south-facing, spaced 8 m apart, and  
135 fixed at an inclination angle of 36°. The panels are mounted 1.7 m and 4.4 m above the  
ground at their lower and upper edges, respectively.

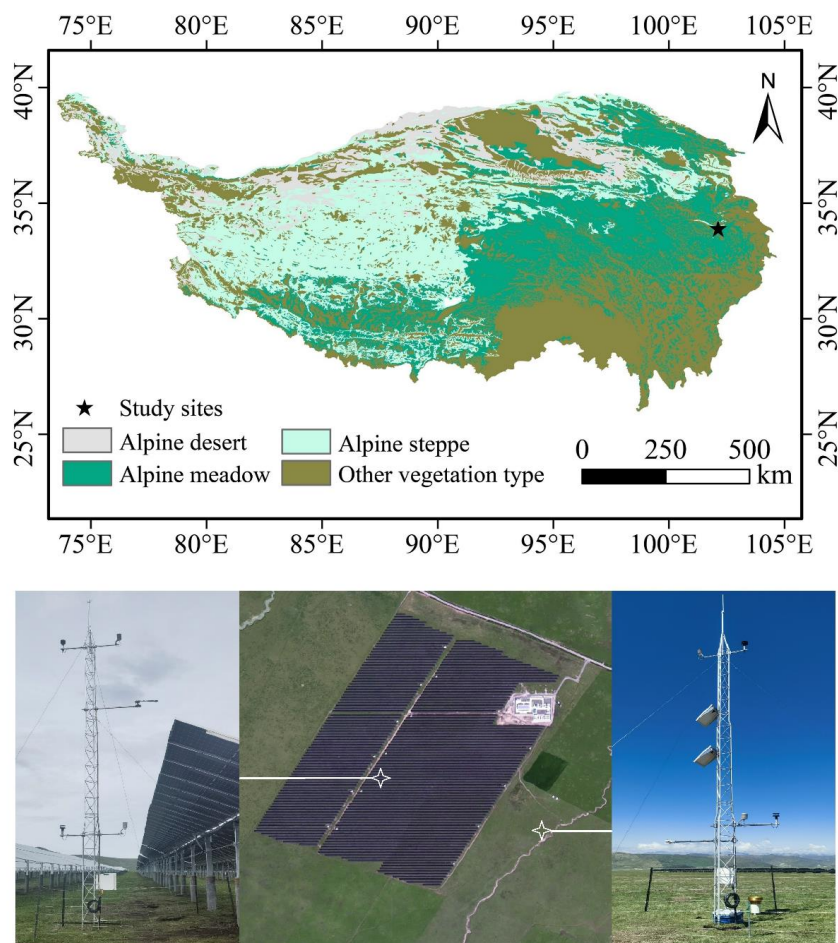


**Figure 01** Map and photographs showing (a) location of Dongneng solar power plant in Tibetan Plateau, (b) © Google map of Dongneng solar power plant and surrounding area, (c) PV measurement site, and (c) reference site.

140

## 2.2 Measurements

This study deployed two 10-m towers (Fig. 01b): one within the PV array (PV site, Fig. 01c) and another reference site (RF site, Figure 01d) in an unmodified alpine meadow, approximately 180 m east of the PV farm. The RF site served as a baseline for comparing environmental conditions in areas impacted by the PV farm. Air temperature and humidity were recorded using HC2A-S3 sensors (Rotronic Instrument Corp., Switzerland) at 2.5 m and 10 m heights on both towers. Wind speed and direction were

145



measured with WindSonic4 sensors (Gill Instruments, UK) at the same heights to  
evaluate the PV array's effect on local airflow patterns. Four-component radiation  
150 measurements (CNR-4, Kipp and Zonen, Netherlands) were taken at 2 m for the RF  
site and at 7 m for the PV site to assess the differences in radiation balance above the  
PV array and over the natural meadow. Soil temperature (CS109, Campbell Scientific,  
Inc., USA) and moisture (CS616, Campbell Scientific, Inc., USA) were measured at  
depths of 5 cm and 10 cm. At the PV site, sensors were installed beneath the PV panels  
155 and in the inter-row gaps to assess the hydrothermal effects of shading. All sensors were  
set to a sampling frequency of 1 Hz, with data averaged every 10 minutes by the  
CR1000 data loggers (Campbell Scientific, Inc., USA). Data were collected  
continuously over a one-year period, from June 2023 to May 2023, to capture seasonal  
variations in microclimate and soil hydrothermal conditions.

160 To ensure data quality, the study applied the following quality control measures: (1) the  
short-wave radiation at night was set to zero according to the solar altitude angle; (2)  
removed downward shortwave radiation exceeding the solar constant ( $1361 \text{ W/m}^2$ )  
during the daytime; (3) used the MAD method (Mauder et al., 2013) for outlier  
detection in temperature and humidity data. If three consecutive outliers were present,  
165 they were not considered as actual anomalies.

### 3. Results and discussion

#### 3.1 The effect of PV arrays on wind regimes

During the observation period, the PV site experienced prevailing winds predominantly  
from the west and southeast (Figure 02). The structured layout of the PV panels  
170 redirected airflow primarily toward the east and west, contrasting with the more  
variable wind directions observed at the RF site. At a height of 2.5 m, beneath the upper  
edge of the PV panels, west and east winds accounted for 48% of total airflow in  
summer and 57% in winter, compared to 38% and 43% at the RF site.

The presence of PV panels increased surface roughness, enhancing frictional drag and  
175 obstructing near-surface wind flow. Consequently, wind speeds at a height of 2.5 m



decreased by 39.1% in spring, 36.0% in summer, 33.6% in fall, and 36.2% in winter. The reduction was most pronounced for southeast winds, exceeding 70%, while the impact on west winds was relatively minor, with wind speed reductions of approximately 30%.

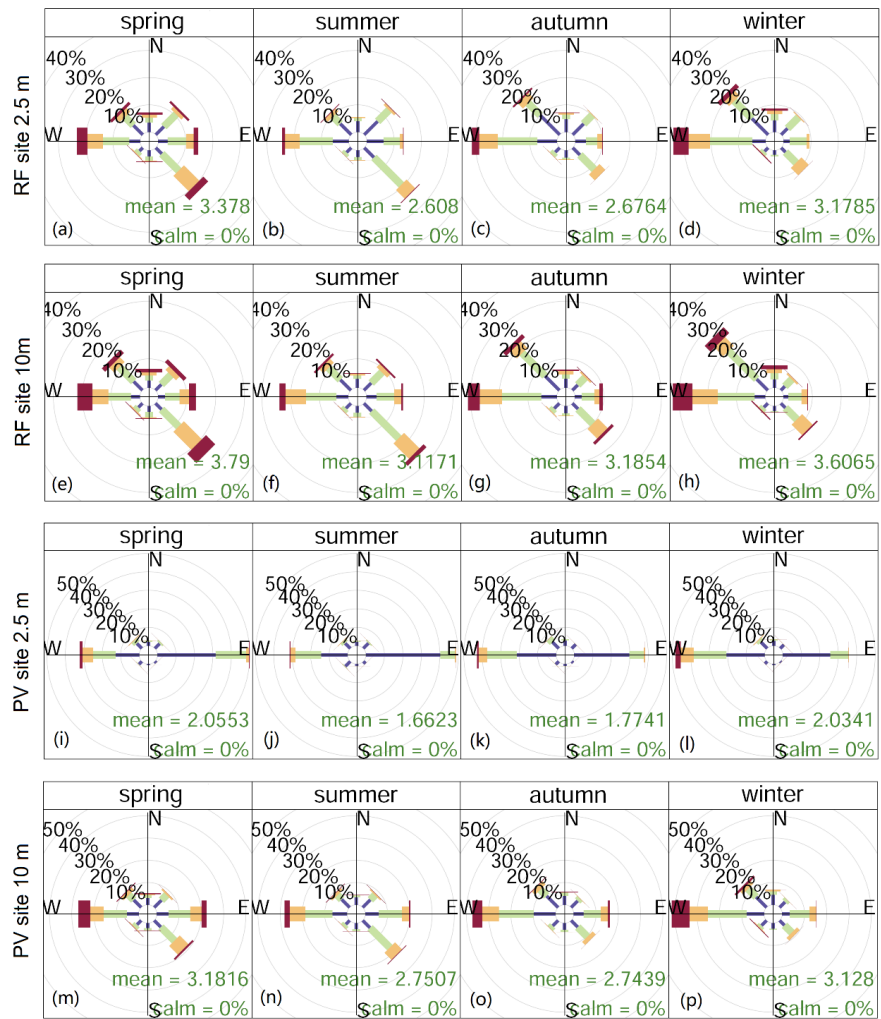


**Figure 02 The wind roses at two comparative sites.**

At 10 m, above the top edge of the PV panels, the directional redistribution of airflow by the panels remained consistent. West and east winds accounted for 48% of the total in summer and 56% in winter, compared to 36% and 40% at the RF site. However, the obstructive effect of the PV panels on wind speed was less pronounced at this height,





with reductions of 15.8% in spring, 11.9% in summer, 14.1% in fall, and 13.3% in winter. North winds experienced the largest reductions (approximately 40%), while west winds were minimally affected, with reductions of around 7%.

These findings reveal a pronounced directional dependence of the PV panels' influence on wind regimes, consistent with previous studies (Jiang et al., 2021; Li et al., 2022b). However, variations in the magnitude of effects can be attributed to differences in PV field layouts and background climatic conditions.

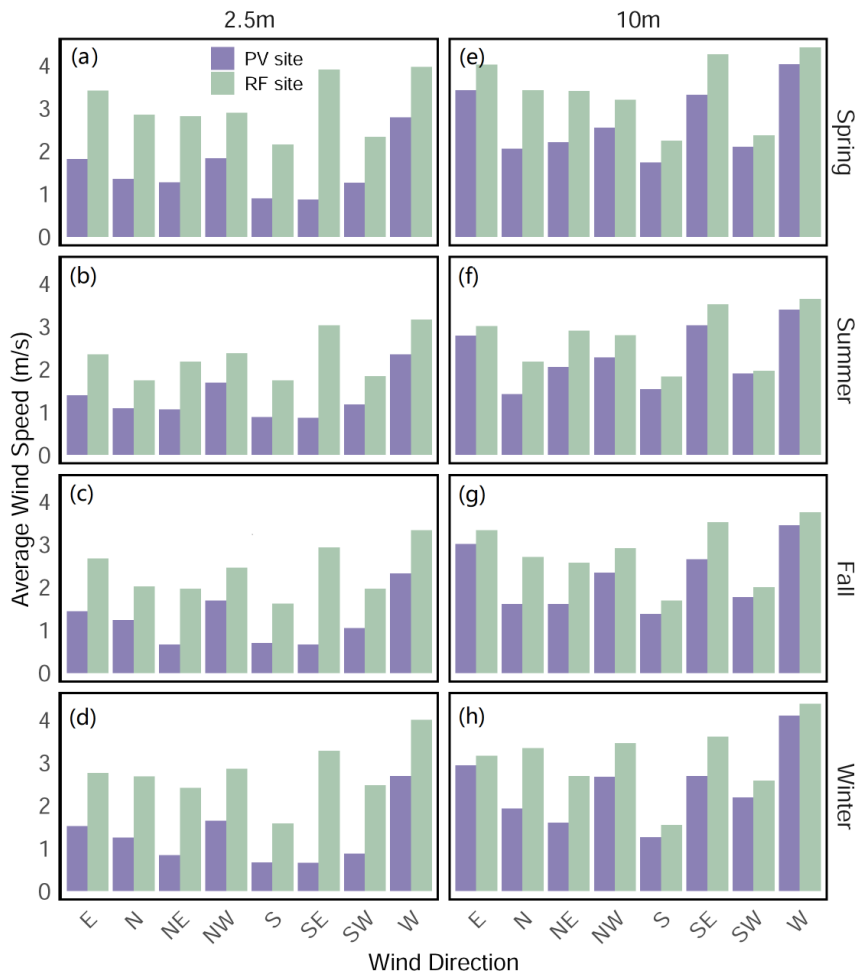


**Figure 03 Seasonal variations in average wind speed by direction at 2.5 m and 10 m heights for PV and RF sites.**



3.2. The effect of PV panels on surface radiation components

As shown in Figure 04 and Table 01, downward shortwave radiation (DR) and downward longwave radiation (DLR) measured above the PV panels were comparable to those observed over the natural meadow. However, upward shortwave radiation (UR) was significantly reduced above the PV panels due to their strong solar absorption, particularly in the peak values of the seasonal average diurnal variations. The peak UR values were approximately 38% lower in summer and 50% lower in winter at the PV site. The daily total UR at the PV site was lower than at the RF site by 36.7% in spring, 36.8% in summer, 43.2% in fall, and 47.8% in winter (Table 01).

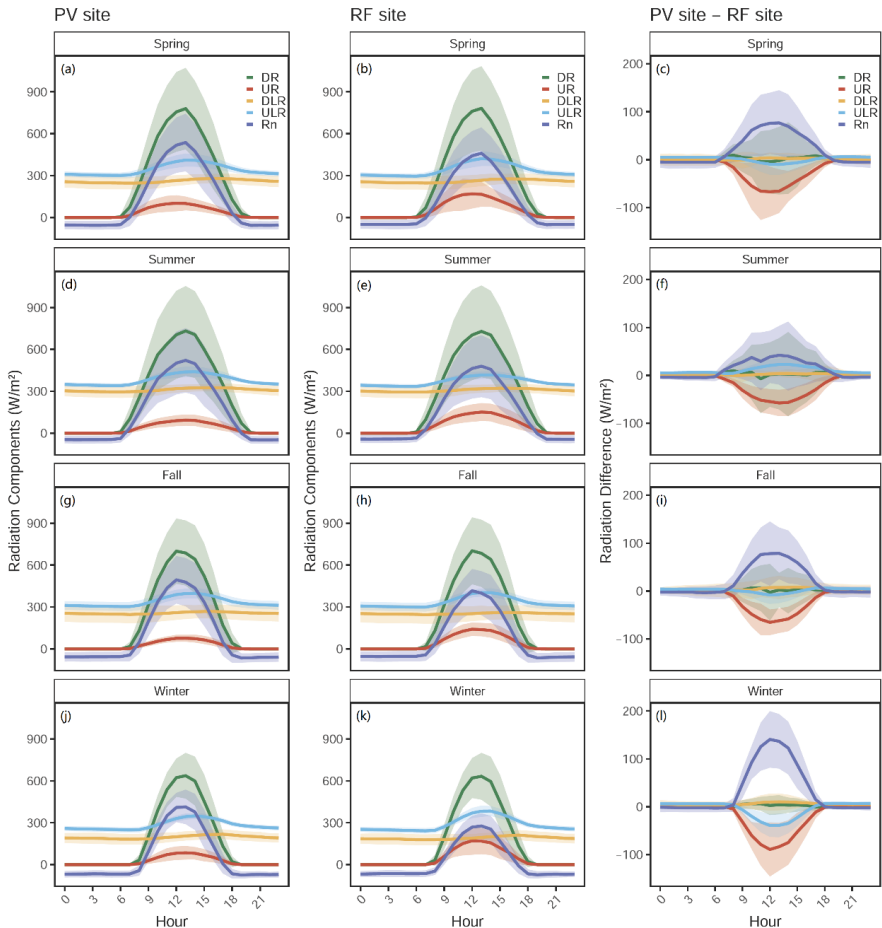


Figure 04 Seasonal averaged diurnal variations in radiation components and their differences between PV and RF sites.



**Table 01 Averaged daily total radiation (MJ) components for PV and RF sites.**

		PV site	RF site	Relative change
DR	Spring	20.48	20.33	0.7
	Summer	20.99	20.82	0.8
	Fall	16.94	16.83	0.6
	Winter	14.12	14.00	0.9
	Annual	18.13	17.99	0.8
UR	Spring	2.93	4.63	-36.7
	Summer	2.85	4.51	-36.8
	Fall	2.04	3.59	-43.2
	Winter	2.04	3.90	-47.8
	Annual	2.46	4.16	-40.8
DLR	Spring	22.54	22.46	0.4
	Summer	26.77	26.59	0.7
	Fall	22.15	21.95	0.9
	Winter	15.94	15.81	0.8
	Annual	21.85	21.70	0.7
ULR	Spring	29.52	29.41	0.4
	Summer	32.12	31.90	0.7
	Fall	29.04	28.88	0.6
	Winter	24.48	24.85	-1.5
	Annual	28.79	28.76	0.1
Rn	Spring	10.56	8.75	20.7
	Summer	12.79	11.00	16.3
	Fall	8.01	6.31	26.8
	Winter	3.55	1.05	238.1
	Annual	8.73	6.78	28.8

210 The daily albedo at the PV site was 0.184 in spring, 0.159 in summer, 0.161 in fall, and  
0.228 in winter. Compared to the RF site, the PV array reduced the albedo by 29.9%,  
33.6%, 33.4%, and 30.1%, respectively. At an annual scale, installation of a PV field  
led to a 31.56% decrease in surface albedo compared to the alpine meadow. As  
summarized in Table 02, the reduction in albedo of this alpine meadow is slightly lower  
215 than the average findings over desert areas at annual and seasonal scales (Broadbent et  
al., 2019; Li et al., 2022c; Stern et al., 2023; Yang et al., 2017; Ying et al., 2023), but  
much higher than that observed over barren areas (Chang et al., 2018) and water body  
(Ying et al., 2023). The reduction in this study aligns with the finding that the higher  
the albedo of the background surface, the more pronounced the relative change in



220 surface albedo over the PV farm (Xu et al., 2024).

For upward longwave radiation (ULR), although the daily cumulative values between the two sites are relatively similar (Table 01), their differences vary between day and night as well as across seasons. During nighttime, ULR at the PV site is consistently slightly higher than that at the RF site across all seasons, with an average increase of  
225 approximately  $5.0 \text{ W m}^{-2}$ . However, during the daytime, seasonal variations showed contrasting patterns. In spring, fall, and winter, the PV site recorded lower ULR than the RF site. The daytime greatest negative deviation being most pronounced in winter ( $-39.0 \text{ W m}^{-2}$ ), followed by spring ( $-10.1 \text{ W m}^{-2}$ ) and autumn ( $-8.0 \text{ W m}^{-2}$ ).

PV plant effects on ULR, which vary between daytime and nighttime as well as across  
230 different seasons, have also been observed in previous studies (Broadbent et al., 2019; Chang et al., 2018; Jiang et al., 2021; Li et al., 2022b; Yang et al., 2017). The underlying reasons for these variations are primarily attributed to three interrelated factors: (1) the lower emissivity of PV modules ( $\sim 0.83$ ) (Broadbent et al., 2019) compared to natural surface ( $0.95\text{--}1$ ) (Campbell and Norman, 1998), which reduce ULR; 2) the cavity effect  
235 (Broadbent et al., 2019), where semi-enclosed spaces beneath PV modules cause repeated radiative exchanges, enhancing ULR; and 3) differences in land surface temperature (LST), which influences ULR patterns depending on the season and time of day (Chang et al., 2018; Yang et al., 2017). Wang et al. (2024b) reported that the PV site exhibited higher land surface temperatures (LST) during nighttime and the warm-  
240 season daytime, but lower LST during the daytime in the cold season. This result suggest that during both nighttime and warm-season daytime, the elevated LST at the PV site exerts a positive influence on ULR, while the reduced LST at the PV site during the cold-season daytime has a negative effect, diminishing ULR.

In this study, we infer that the higher ULR observed at the PV site during both nighttime  
245 and summer daytime is primarily due to the combined positive effects of the cavity effect and the higher LST, which outweigh the negative effect of the PV modules' lower emissivity. Conversely, the lower ULR at the PV site compared to the reference site during the daytime in spring, autumn, and winter likely results from the dominant negative effects of lower LST and the PV modules' lower emissivity, which surpass the



250 positive effect of the cavity effect.

The net radiation ( $R_n$ ) differences between the PV and RF sites also showed clear seasonal dependencies. The PV site exhibited higher  $R_n$  across all seasons, with peak diurnal variations exceeding the RF site by  $76.8 \text{ Wm}^{-2}$  in spring,  $42.0 \text{ Wm}^{-2}$  in summer,  $78.8 \text{ Wm}^{-2}$  in fall, and  $140.6 \text{ Wm}^{-2}$  in winter. The relative difference in  $R_n$  between two sites also showed that the influence of PV panels on  $R_n$  was most pronounced in winter (Table 01), corresponds to the result that the largest relative difference in albedo during this season. Consistent with previous studies (Broadbent et al., 2019; Chang et al., 2018; Jiang et al., 2021; Li et al., 2022b; Li et al., 2022c), PV modules can significantly amplify land surface energy availability. The relative difference in  $R_n$  between our two sites showed that the influence of PV panels on  $R_n$  was most pronounced in winter (Table 01), not only due to the largest relative difference in albedo during this season but also as a result of manual adjustments to the tilt angle of PV panels and snow clearing on their surfaces.

**Table 02 Comparison of in-situ albedo observations across different PV power plant.**

Latitude (°)	Longitude (°)	Land cover	In-situ albedo observations			Source
			Background	Absolute change	Relative change	
36.136N	100.588E	Barren	0.17 <sup>Summer</sup>	-0.01	-6.3%	Chang et al. (2018)
36.136N	100.588E	Barren	0.19 <sup>Winter</sup>	0.02	11%	Chang et al. (2018)
36.503N	95.233E	Desert	0.26 <sup>Annual</sup>	-0.07	-27%	Yang et al. (2017)
44.410N	87.660E	Desert	0.23 <sup>Summer</sup>	-0.09	-39.1%	Li et al. (2022c)
44.410	87.660E	Desert	0.22 <sup>Summer</sup>	-0.08	-36.4%	Ying et al. (2023)
29.965N	35.059E	Desert	0.38 <sup>Annual</sup>	-0.21	-55.2%	Stern et al.



						(2023)
32.555N	111.284°W	Desert	0.31 <sup>October to</sup>	-0.11	-35.5%	Broadbent et al.
			June			(2019)
32.303N	119.793E	Water	0.101 <sup>annual</sup>	-0.019	-18.8%	Li et al. (2022b)
		body				
34.055N	101.888E	Alpine	0.184 <sup>Spring</sup>	-0.079	-29.9%	This study
		meadow				
34.055N	101.888E	Alpine	0.159 <sup>Summer</sup>	-0.081	-33.6%	This study
		meadow				
34.055N	101.888E	Alpine	0.161 <sup>Fall</sup>	-0.081	-33.4%	This study
		meadow				
34.055N	101.888E	Alpine	0.228 <sup>Winter</sup>	-0.098	-30.1%	This study
		meadow				
34.055N	101.888E	Alpine	0.258 <sup>annual</sup>	-0.085	-31.6%	This study
		meadow				

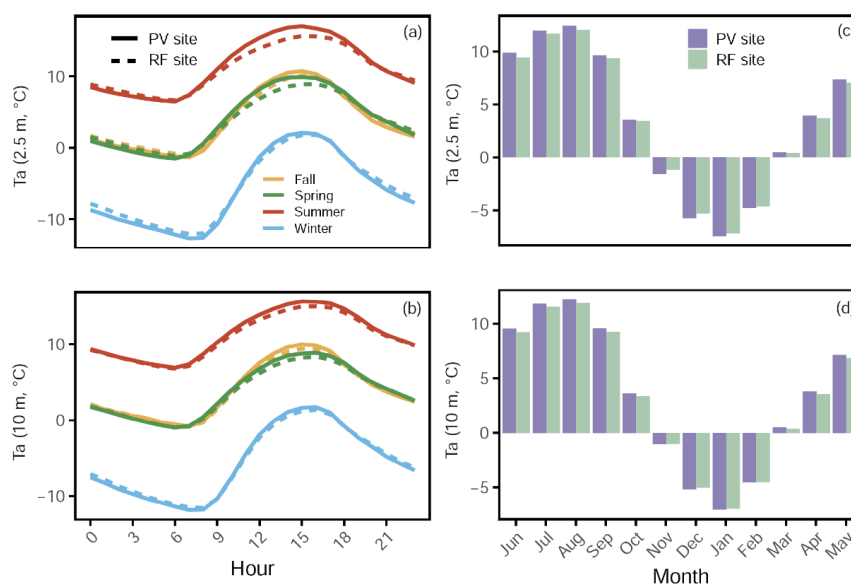
---



### 265 3.3 The effect of PV arrays on air temperature and humidity

The PV panels significantly influenced air temperature ( $T_a$ ) at both 2.5 m and 10 m heights, with diurnal and seasonal variations observed between the PV site and RF site (Figure 05). At 2.5 m, the PV site exhibited an average annual  $T_a$  increase of  $0.08^\circ\text{C}$  compared to the RF site. This increase was more pronounced at 10 m, with an annual mean difference of  $0.17^\circ\text{C}$ .

The influence of PV panels on  $T_a$  demonstrated a distinct diurnal asymmetry. During the daytime, the PV site consistently shows a warm bias relative to the RF site due to heat released from PV panels. The maximum warm bias ranges from  $0.65^\circ\text{C}$  (winter) to  $1.60^\circ\text{C}$  (summer) at 2.5 m, and from  $0.46^\circ\text{C}$  (winter) to  $0.70^\circ\text{C}$  (summer) at 10 m. These values are consistent with previous studies in desert or barren areas, which reported local increases in daytime air temperature ranging from  $0.1^\circ\text{C}$  to  $1.9^\circ\text{C}$  (Broadbent et al., 2019; Fthenakis and Yu, 2013; Jiang et al., 2021; Yang et al., 2017).



280 **Figure 05 Diurnal and monthly variations of air temperature ( $T_a$ ) at different heights (2.5 m and 10 m) for PV and RF sites.**

During the nighttime, the PV site exhibits a cold bias relative to the RF site. At 2.5 m, the maximum cold bias ranges from  $-0.46^\circ\text{C}$  in summer to  $-0.89^\circ\text{C}$  in winter, while at



10 m, it varies between  $-0.01^{\circ}\text{C}$  in summer and  $-0.46^{\circ}\text{C}$  in winter. The cooling effect of PV farms is primarily attributed to two key mechanisms (Barron-Gafford et al., 2016; Broadbent et al., 2019; Yang et al., 2017): (1) the shielding effect of PV panels, which minimizes heat accumulation in the soil and enhances nocturnal radiative cooling of the ground surface; and (2) the reduction in PV panel temperatures below ambient air temperature at night, further contributing to the cooling of near-surface air. Interestingly, a small number of studies have reported that PV plants also exhibit a nocturnal warming effect. For instance, Barron-Gafford et al. (2016) observed a significant nocturnal heating effect of  $3\text{--}4^{\circ}\text{C}$  at a height of 2.5 m in a utility-scale PV array in southern Arizona. This may be attributed to the presence of impervious surfaces near the PV array, as well as the smaller and less continuous scale of the PV array (Broadbent et al., 2019).

The dynamics of monthly  $T_a$  suggest that PV panels also exhibit asymmetrical effects on near-surface air temperature between warm and cold seasons (Figure 05c, d). From March to October, the PV site generally experiences higher  $T_a$  than the RF site. However, from November to February, the PV site sees lower  $T_a$  compared to the RF site. This seasonal reversal may be attributed to the enhanced cooling effect and reduced warming effect of PV panels during the colder months with lower solar input.

The warming effect of PV arrays on  $T_a$  in this alpine meadow region is much weaker than that observed in low-altitude areas (Barron-Gafford et al., 2016; Fthenakis and Yu, 2013; Jiang et al., 2021; Li et al., 2022b; Yang et al., 2017). This phenomenon can be attributed not only to differences in PV array characteristics but, more importantly, to the lower background temperature in this region. Higher daily temperatures are known to enhance the warming effect of PV panels (Broadbent et al., 2019; Jiang et al., 2021). Specific humidity ( $q$ ) was also influenced by the PV panels. It was consistently higher than at the RF site (Figure 06). This increase was most significant during summer daytime, when  $q$  at the PV site was up to 4% higher at a height of 2.5 m. This can be attributed to reduced wind speeds and lower evapotranspiration beneath the PV panels, which retain more moisture in the immediate environment. At 10 m, however, the differences in  $q$  between the two sites were less pronounced due to the reduced





influence of near-surface shading.

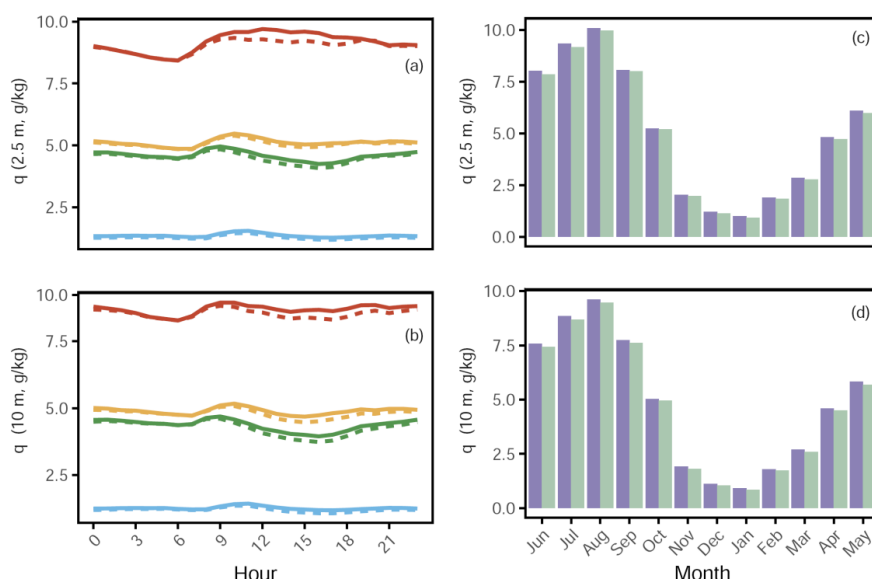


**Figure 06 Diurnal and monthly variations of air specific humidity ( $q$ ) at different heights (2.5 m and 10 m) for PV and RF sites.**

The vapor pressure deficit (VPD) exhibits diurnal and seasonal patterns (Figure 07) similar to those of  $T_a$  (Figure 05). The daytime maximum positive bias ranges from 0.03 kPa (winter) to 0.16 kPa (summer) at 2.5 m, and from 0.01 kPa (winter) to 0.05 kPa (summer) at 10 m. The nighttime maximum negative bias occurs in spring, with a value less than 0.03 kPa. On a seasonal scale, the difference in VPD between the two sites reaches its peak in summer, with the average VPD at 2.5 m and 10 m at the PV site being approximately 10.8% and 4.1% higher than at the RF site, respectively. Annually, VPD at the PV site is slightly higher than at the RF site, with differences of about 5% at 2.5 m and 1% at 10 m.

The discrepancy between VPD and  $q$  suggests that variations in VPD are primarily driven by temperature changes rather than differences in specific humidity in this alpine region. This indicates that, despite the higher  $q$  at the PV site, the warming effect of PV panels during the daytime elevates the air's evaporative demand, potentially exacerbating water loss from vegetation and soil. However, the relatively higher soil moisture observed at the PV site may help offset this effect by sustaining local



evaporation and transpiration rates.

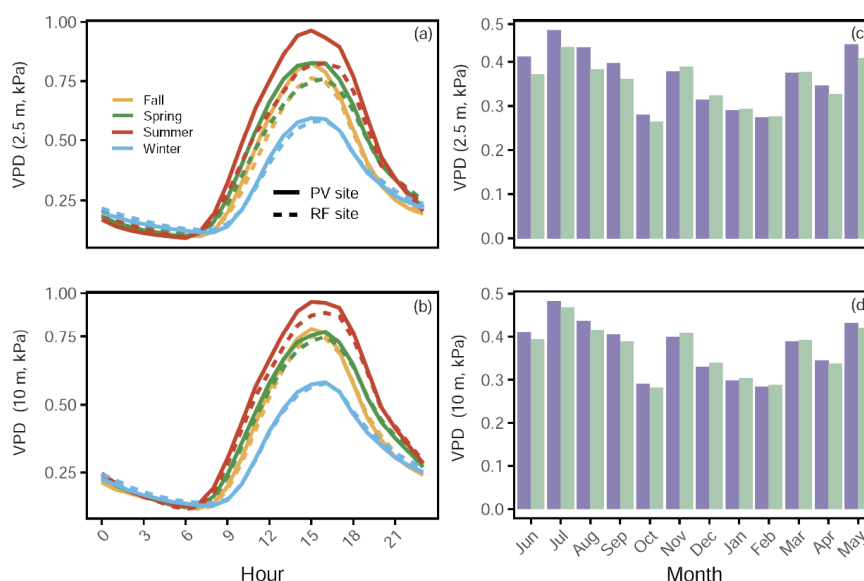


**Figure 07** Diurnal and monthly variations of vapor pressure deficit (VPD) at different heights (2.5 m and 10 m) for PV and RF sites.

### 3.4. The effect of PV arrays on soil temperature and soil moisture

The presence of PV arrays significantly influences the thermal properties of the soil. The shading effect of PV panels results in consistently lower soil temperatures ( $T_s$ ) beneath the panels and in the gaps between rows throughout the year. Soil beneath the panels begin to freeze (daily  $T_s$  below  $0^\circ\text{C}$  for three consecutive days) 27 days earlier and thaw 20 days later compared to the RF site. In the gaps between rows, freezing begins 20 days earlier and thawing is delayed by 31 days. At a 10 cm depth, similar trends are observed, with freezing starting 28 days earlier and thawing delayed by 31 days beneath the panels, and in the gaps, freezing occurs 26 days earlier with a 28-day delay in thawing.

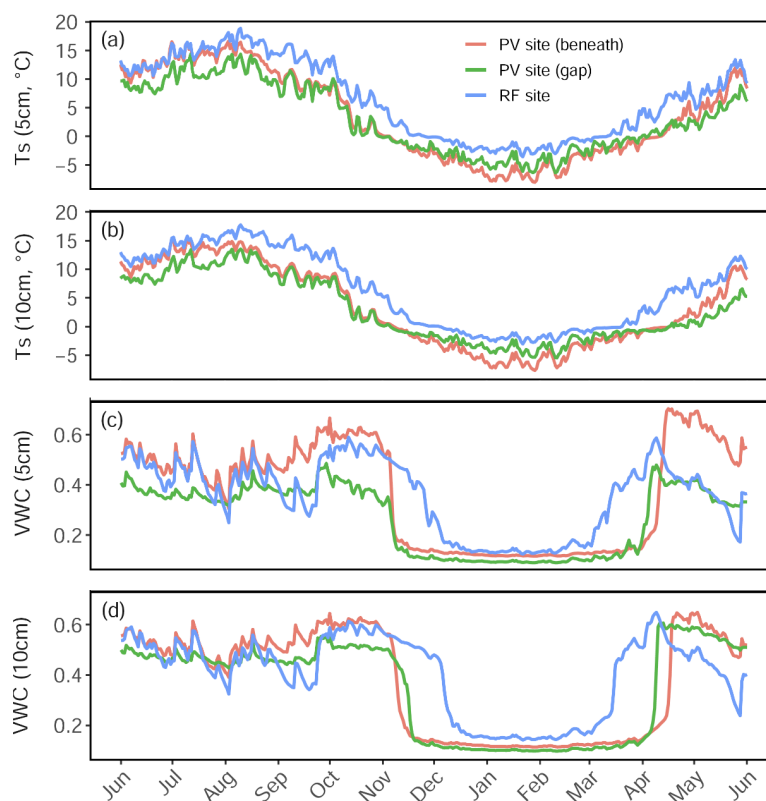


**Figure 08** Seasonal dynamics of daily average soil temperature (Ts) and volumetric water content (VWC) at 5 cm and 10 cm depths.

During spring, summer, and fall, Ts at both depths are highest at the RF site, followed  
 350 by the gaps between the rows, and lowest beneath the panels (Table 03). The differences  
 in Ts between the locations are most pronounced in the fall, with the RF site showing  
 that Ts is 3.89°C higher than in the gaps and 4.23°C higher than beneath the panels at a  
 depth of 5 cm. This result aligns with previous studies that have documented significant  
 cooling effects in PV fields due to shading, which lowers the soil temperature relative  
 355 to surrounding areas (Armstrong et al., 2016; Choi et al., 2024; Wu et al., 2022; Yue et  
 al., 2021; Zheng et al., 2023).

During winter, the Ts pattern shifts to RF site > beneath the panels > in the gaps between  
 the rows (Table 03). Specifically, at a 5 cm depth, the average Ts at the RF site is  
 approximately 2.33°C higher than beneath the panels and 3.83°C higher than in the



gaps. At 10 cm depth, the temperature difference is approximately 1.89°C higher at the RF site compared to beneath the panels, and 3.65°C higher compared to the gaps. The slightly higher  $T_s$  beneath the PV panels compared to the gaps may be attributed to the insulation effect of the panels and their thermal radiation properties. PV panels reduce direct exposure to cold air, limiting heat loss from the soil. Additionally, the panels absorb solar radiation and transfer some of the heat to the soil beneath, helping to maintain relatively higher temperatures. In contrast, the soil in the gaps between the rows is more exposed to cold air, leading to greater temperature fluctuations and lower overall temperatures. (Yue et al., 2021) also reported that the soil beneath the PV panels maintains warmer soil conditions in winter due to the insulation and heat transfer provided by the PV panels.

**Table 03 Average soil temperature (°C) at 5 cm and 10 cm depths for PV and RF sites.**

	Annual	Spring	Summer	Fall	Winter
RF site (5cm)	6.50	5.29	14.64	7.73	-1.67
PV site (gap, 5cm)	3.53	2.24	13.50	3.89	-5.50
PV site (beneath, 5cm)	2.97	1.65	10.73	3.50	-4.00
RF site (10cm)	6.37	4.66	14.37	7.95	-1.49
PV site (gap, 10cm)	3.27	1.53	12.61	4.08	-5.14
PV site (beneath, 10cm)	2.79	0.48	10.42	3.59	-3.34

Soil volumetric water content (VWC) also exhibits significant seasonal variations across different locations (Figure 08). In spring and autumn, soil moisture at the RF site remains consistently higher compared to the other two locations (Table 04). This is primarily due to earlier soil thawing in spring and delayed freezing in autumn at the RF site. In summer, average SWC in gaps between the PV rows is higher than that at the RF site by about 9% at both depths (Table 04). This difference can be mainly attributed to two main factors: (1) the inclined structure of the PV panels channels precipitation toward the gaps between the rows, significantly enhancing water recharge in this area;



(2) the lower wind speed and reduced soil temperature within gaps between the rows, caused by shading from the PV panels, effectively suppress evaporation and maintain higher soil moisture levels. This result align with Choi et al. (2024), who reported that the interspace of PV arrays had the highest soil moisture (25 cm) regardless of whether the PV was bare or vegetated across three utility-scale PV facilities in Minnesota, USA.

**Table 4 Average soil moisture at 5 cm and 10 cm depths for PV and RF sites.**

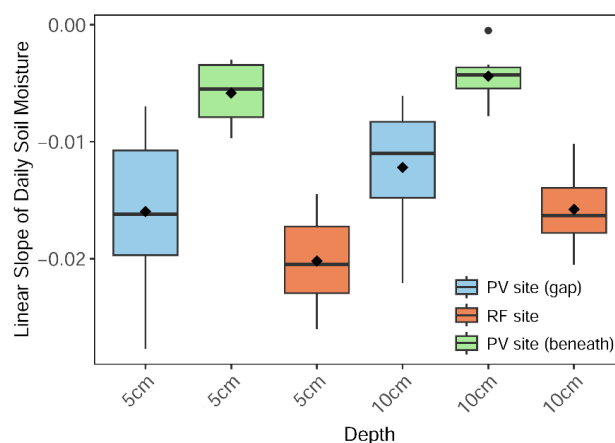
	Annual	Spring	Summer	Fall	Winter
RF site (5cm)	0.36	0.38	0.44	0.46	0.15
PV site (gap, 5cm)	0.37	0.41	0.48	0.45	0.12
PV site (beneath, 5cm)	0.27	0.29	0.37	0.32	0.10
RF site (10cm)	0.40	0.44	0.47	0.51	0.18
PV site (gap, 10cm)	0.37	0.36	0.51	0.48	0.12
PV site (beneath, 10cm)	0.35	0.38	0.47	0.43	0.10

Conversely, the summer average SWC beneath the PV panels is the lowest among the three locations (Table 04) due to precipitation interception by the panels, which limits direct water input to the underlying soil. Interestingly, at 10 cm depth, the summer average SWC shows no significant difference between the beneath-PV and RF sites. However, at 5 cm depth, the SWC beneath PV is approximately 16% lower than at the RF site. This suggests that subsurface soil layers under PV panels may benefit from lateral water redistribution and upward soil moisture migration driven by capillary action and vegetation root water uptake (Jury and Horton, 2004), partially offsetting the reduced surface recharge. Different from the result of Yue et al. (2021), who reported significantly higher SWC at depths of 10–40 cm beneath PV panels compared to non-PV areas during the rainy season, with the moisture difference decreasing with depth. Choi et al. (2024) observed inconsistent effects across facilities: the median SWC beneath PV panels was lower than the reference site in two facilities but higher in one. This highlights that, even under similar climatic conditions, variations in PV system



structure, soil properties, and management practices can lead to inconsistent SWC  
405 patterns beneath PV panels.

Due to the seasonal variability of precipitation, seven consecutive 6-day periods without rainfall occurred in this alpine meadow when the soil was in a thawed state. Therefore, the linear decrease slopes of daily SWC at different locations inside and outside the PV field were compared. The Figure 09 shows that the decrease rates of soil  
410 moisture at the RF site at 5 cm and 10 cm depths are significantly higher than those at PV sites, approximately 1.3 times and 3.5 times the rate of decrease between the PV rows and beneath PV, respectively. This result further indicates that the presence of the PV field effectively inhibits soil moisture loss.



415 **Figure 09 Linear decrease slopes of daily SWC (5cm and 10cm) at different locations for PV and RF sites during dry periods.**

#### 4. Conclusions and Implications

Pastoral-integrated PV power plant, a form of agrivoltaism, offer an innovative solution to the increasing demand for sustainable pastoralism and renewable energy. As solar  
420 PV energy development continues to expand, concerns about its potential impacts on the ecological environment, particularly in fragile and sensitive regions such as the Tibetan Plateau, are gaining prominence.

This study investigates the effects of PV arrays on the local meteorological conditions and soil hydrothermal dynamics in a high-altitude alpine meadow on the eastern Tibetan



425 Plateau. The findings reveal that the installation of PV panels increases annual mean  
net radiation by 28.9%, while reducing albedo and 2.5 m wind speed by 31.6% and  
36.2%, respectively. Despite the slight warming effect on annual mean air temperature  
(Ta), the impact of PV panels is highly asymmetric: daytime heating, nighttime cooling,  
summer warming, and winter cooling. During summer daytime, Ta, q, and VPD at the  
430 PV site are 11.1%, 4%, and 22.2% higher, respectively, than at the RF site. The PV field  
introduces substantial spatial heterogeneity in soil hydrothermal properties. Beneath the  
panels, the soil exhibits a cold-moist characteristic, while the gaps between PV rows  
display a cold-dry distribution. Lower soil temperatures extend the frozen period within  
the PV field by nearly 50 days compared to the RF site. Furthermore, the rate of soil  
435 moisture loss during non-freezing periods is significantly reduced, with depletion rates  
beneath the panels and in the gaps being up to 3.5 and 1.3 times lower, respectively,  
compared to the RF site.

These results suggest that PV arrays provide thermal buffering effects, which are crucial  
for mitigating the impacts of climate warming on the Tibetan Plateau. Climate  
440 projections indicate that global temperatures will likely surpass the 1.5 °C threshold,  
with regional warming on the Tibetan Plateau expected to exceed the global average  
due to elevation-dependent warming (You et al., 2020). Such rapid warming has already  
impacted soil freeze-thaw cycles, hydrological systems, carbon dynamics, and  
vegetation succession (Armstrong et al., 2014; Chen et al., 2022; Luo et al., 2020; Ma  
445 et al., 2022; Yang et al., 2014; Zhao et al., 2021). By buffering soil temperature  
fluctuations and extending the frozen period, PV arrays can mitigate permafrost  
degradation and associated greenhouse gas emissions. Moreover, reduced soil moisture  
depletion during dry periods creates favorable conditions for vegetation growth and  
photosynthesis. However, the shortened growing season may reduce vegetation carbon  
450 absorption, potentially offsetting some of these benefits.

The study area, a critical water source region for the upper Yellow River, plays a vital  
role in regional hydrology. Enhanced soil moisture promotes deep percolation, which  
strengthens groundwater recharge and supports water conservation. However, changes  
in freeze-thaw dynamics, such as advanced freezing and delayed thawing, could alter



455 the spatial and temporal distribution of runoff. This is particularly evident in the release  
patterns of meltwater and frozen soil water, potentially disrupting downstream water  
availability. Although the current observational equipment in this study does not  
provide quantitative evapotranspiration (ET) results, an analysis based on the  
established relationship between ET and meteorological factors (Allen et al., 1998)  
460 indicates that PV arrays exert a dual impact on ET. On one hand, PV systems elevate  
Ta and VPD, which enhances atmospheric demand for water vapor, thereby intensifying  
ET. On the other hand, the shading effect of PV panels reduces the Rn reaching the soil  
surface, and the structural design of the arrays significantly decreases wind speed.  
These two factors collectively suppress ET. Therefore, subsequent research should  
465 utilize eddy covariance systems, along with lysimeters, to quantitatively assess the  
impact of PV fields on ET.

From a biodiversity perspective, the introduction of microenvironmental heterogeneity  
through shading and moisture redistribution by PV arrays may influence vegetation  
dynamics. The reduced Ts and longer frozen conditions may limit the dominance of tall,  
470 light-demanding grasses, creating niches for shade-tolerant C3 plants (Wang et al.,  
2024a). This shift could counteract vegetation homogenization trends, promoting  
species diversity in alpine grasslands. However, the shortened growing season poses  
challenges for species with growth cycles tied to freeze-thaw dynamics, potentially  
reducing their adaptive capacity. PV arrays may act as both stabilizing and destabilizing  
475 forces for plant communities, necessitating further study on their long-term ecological  
impacts.

These broader-scale implications suggest that PV arrays offer a pathway to improve  
alpine meadow ecosystem resilience in a warming climate. Future research should  
incorporate multi-year observations and numerical models to evaluate the long-term  
480 effects of PV arrays on regional climate, hydrological processes, and ecological  
functions, including biodiversity and carbon sequestration, under varying climatic  
conditions.





### **Code/Data availability**

485 The data and code supporting the findings of this study are available upon request to the corresponding author, Shaoying Wang (wangshaoying@lzb.ac.cn).

### **Author contribution**

Conceptualization: SW and XM; methodology: SW, PY and QL; funding acquisition: SW, XM, ZL and ZL; data curation and visualization: SW, LS, and WN; field measurement: SW, WN; All authors actively contributed to the discussions and to the writing of the final version of the paper.

### **Competing interests**

The contact author has declared that none of the authors has any competing interests.

### **Acknowledgments**

495 The authors would like to thank the Zoige Plateau Wetland Ecosystem Research Station for providing the observation equipment used in this study. We are also deeply grateful to the editor and reviewers for their constructive comments, which greatly improved the quality of this paper.

### **Financial support**

500 This study was supported by the National Science Fund for Distinguished Young Scholars of China (42325502), the Key Project of Gansu Province Science and Technology Plan (23ZDFA011), the National Natural Science Foundation of China (41875018), the Science and Technology Research Plan of Gansu Province (22JR5RA048), and the Ningxia Hui Autonomous Region Key Research and Development Program (2024BEG03003).

505

### **References**

Allen, R.G., Pereira, L.S., Raes, D. and Smith, M., 1998. Crop evapotranspiration - Guidelines for computing crop water requirements - FAO Irrigation and drainage paper 56. FAO Rome, 300(9):



- D05109.
- 510 Armstrong, A., Ostle, N.J. and Whitaker, J., 2016. Solar park microclimate and vegetation management effects on grassland carbon cycling. *Environmental Research Letters*, 11(7): 074016.
- Armstrong, A., Waldron, S., Whitaker, J. and Ostle, N.J., 2014. Wind farm and solar park effects on plant–soil carbon cycling: uncertain impacts of changes in ground-level microclimate. *Global Change Biology*, 20(6): 1699-1706.
- 515 Barron-Gafford, G.A. et al., 2016. The Photovoltaic Heat Island Effect: Larger solar power plants increase local temperatures. *Scientific Reports*, 6(1): 35070.
- Birol, F., 2022. *World Energy Outlook 2022*. International Energy Agency: Paris, France, 522.
- Broadbent, A.M., Krayenhoff, E.S., Georgescu, M. and Sailor, D.J., 2019. The observed effects of utility-scale photovoltaics on near-surface air temperature and energy balance. *Journal of Applied Meteorology and Climatology*, 58(5): 989-1006.
- 520 Campbell, G.S. and Norman, J.M., 1998. *Radiation Basics*. In: G.S. Campbell and J.M. Norman (Editors), *An Introduction to Environmental Biophysics*. Springer New York, New York, NY, pp. 147-165.
- Chang, R. et al., 2018. Observed surface radiation and temperature impacts from the large-scale deployment of photovoltaics in the barren area of Gonghe, China. *Renewable Energy*, 118: 131-137.
- 525 Chen, H. et al., 2022. Carbon and nitrogen cycling on the Qinghai–Tibetan Plateau. *Nature Reviews Earth & Environment*, 3(10): 701-716.
- Chen, L. et al., 2016. Determinants of carbon release from the active layer and permafrost deposits on the Tibetan Plateau. *Nature Communications*, 7(1): 13046.
- 530 Choi, C.S., Macknick, J., McCall, J., Bertel, R. and Ravi, S., 2024. Multi-year analysis of physical interactions between solar PV arrays and underlying soil-plant complex in vegetated utility-scale systems. *Applied Energy*, 365: 123227.
- Fthenakis, V. and Yu, Y., 2013. Analysis of the potential for a heat island effect in large solar farms, 2013 IEEE 39th Photovoltaic Specialists Conference (PVSC). IEEE, pp. 3362-3366.
- 535 Jiang, J., Gao, X., Lv, Q., Li, Z. and Li, P., 2021. Observed impacts of utility-scale photovoltaic plant on local air temperature and energy partitioning in the barren areas. *Renewable Energy*, 174: 157-169.
- Jury, W.A. and Horton, R., 2004. *Soil physics*. John Wiley & Sons.
- Kan, A. et al., 2021. The linkage between renewable energy potential and sustainable development: Understanding solar energy variability and photovoltaic power potential in Tibet, China. *Sustainable Energy Technologies and Assessments*, 48: 101551.
- 540 Keiko, S., SINHA, S., Birendra, K. and KOJIMA, T., 2009. Self Cooling Mechanism in Photovoltaic Cells and Its Impact on Heat Island Effect from Very Large Scale PV Systems in Deserts. *Journal of Arid Land Studies*, 19( 1): 5-8.
- 545 Li, M. et al., 2022a. High-resolution data shows China’s wind and solar energy resources are enough to support a 2050 decarbonized electricity system. *Applied Energy*, 306: 117996.
- Li, P., Gao, X., Li, Z., Ye, T. and Zhou, X., 2022b. Effects of fishery complementary photovoltaic power plant on near-surface meteorology and energy balance. *Renewable Energy*, 187: 698-709.
- Li, Y. et al., 2018. Climate model shows large-scale wind and solar farms in the Sahara increase rain and vegetation. *Science*, 361(6406): 1019-1022.
- 550 Li, Z. et al., 2022c. A comparative study on the surface radiation characteristics of photovoltaic power plant in the Gobi desert. *Renewable Energy*, 182: 764-771.



- Lu, Z. et al., 2021. Impacts of Large-Scale Sahara Solar Farms on Global Climate and Vegetation Cover. *Geophysical Research Letters*, 48(2): e2020GL090789.
- 555 Luo, S., Wang, J., Pomeroy, J.W. and Lyu, S., 2020. Freeze–Thaw Changes of Seasonally Frozen Ground on the Tibetan Plateau from 1960 to 2014. *Journal of Climate*, 33(21): 9427–9446.
- Lyu, X. et al., 2024. Mapping of Utility-Scale Solar Panel Areas From 2000 to 2022 in China Using Google Earth Engine. *IEEE Journal of Selected Topics in Applied Earth Observations and Remote Sensing*, 17: 18083–18095.
- 560 Ma, L. et al., 2022. Warming changed the relationship between species diversity and primary productivity of alpine meadow on the Tibetan Plateau. *Ecological Indicators*, 145: 109691.
- Mauder, M. et al., 2013. A strategy for quality and uncertainty assessment of long-term eddy-covariance measurements. *Agricultural and Forest Meteorology*, 169: 122–135.
- Průvák, R., Patriche, C. and Bandoc, G., 2019. Spatial assessment of solar energy potential at global scale. A geographical approach. *Journal of Cleaner Production*, 209: 692–721.
- 565 Stern, R. et al., 2023. Photovoltaic fields largely outperform afforestation efficiency in global climate change mitigation strategies. *PNAS Nexus*, 2(11): pgad352.
- Taha, H., 2013. The potential for air-temperature impact from large-scale deployment of solar photovoltaic arrays in urban areas. *Solar Energy*, 91: 358–367.
- 570 Tang, W., Yang, K., Qin, J. and Min, M., 2013. Development of a 50-year daily surface solar radiation dataset over China. *Science China Earth Sciences*, 56(9): 1555–1565.
- Wang, L. et al., 2024a. Drivers of plant diversification along an altitudinal gradient in the alpine desert grassland, Northern Tibetan Plateau. *Global Ecology and Conservation*, 53: e02987.
- Wang, Q. and Qiu, H.-N., 2009. Situation and outlook of solar energy utilization in Tibet, China. *Renewable and Sustainable Energy Reviews*, 13(8): 2181–2186.
- 575 Wang, X. et al., 2024b. Diurnal Asymmetry Effects of Photovoltaic Power Plants on Land Surface Temperature in Gobi Deserts, *Remote Sensing*.
- Wei, S. et al., 2024. Small reduction in land surface albedo due to solar panel expansion worldwide. *Communications Earth & Environment*, 5(1): 474.
- 580 Wu, C. et al., 2022. Ecohydrological effects of photovoltaic solar farms on soil microclimates and moisture regimes in arid Northwest China: A modeling study. *Science of The Total Environment*, 802: 149946.
- Xu, Z., Li, Y., Qin, Y. and Bach, E., 2024. A global assessment of the effects of solar farms on albedo, vegetation, and land surface temperature using remote sensing. *Solar Energy*, 268: 112198.
- 585 Yang, K. et al., 2014. Recent climate changes over the Tibetan Plateau and their impacts on energy and water cycle: A review. *Global and Planetary Change*, 112: 79–91.
- Yang, L. et al., 2017. Study on the local climatic effects of large photovoltaic solar farms in desert areas. *Solar Energy*, 144: 244–253.
- Yao, T. et al., 2022. The imbalance of the Asian water tower. *Nature Reviews Earth & Environment*, 3(10): 618–632.
- 590 Ying, J. et al., 2023. The characteristics and parameterizations of the surface albedo of a utility-scale photovoltaic plant in the Gobi Desert. *Theoretical and Applied Climatology*, 151(3): 1469–1481.
- You, Q. et al., 2020. Tibetan Plateau amplification of climate extremes under global warming of 1.5 °C, 2 °C and 3 °C. *Global and Planetary Change*, 192: 103261.
- 595 Yue, S., Guo, M., Zou, P., Wu, W. and Zhou, X., 2021. Effects of photovoltaic panels on soil temperature and moisture in desert areas. *Environmental Science and Pollution Research*, 28: 17506–17518.



Zhao, D., Zhu, Y., Wu, S. and Zheng, D., 2021. Projection of vegetation distribution to 1.5 °C and 2 °C of global warming on the Tibetan Plateau. *Global and Planetary Change*, 202: 103525.

600 Zheng, J., Luo, Y., Chang, R. and Gao, X., 2023. An observational study on the microclimate and soil thermal regimes under solar photovoltaic arrays. *Solar Energy*, 266: 112159.